

Accepted Manuscript

Fragment-based discovery of novel pentacyclic triterpenoid derivatives as cholesteryl ester transfer protein inhibitors

Yongzhi Chang, Shuxi Zhou, Enqin Li, Wenfeng Zhao, Yanpeng Ji, Xiaoran Wen, Hongbin Sun, Haoliang Yuan



PII: S0223-5234(16)30861-3

DOI: [10.1016/j.ejmech.2016.09.098](https://doi.org/10.1016/j.ejmech.2016.09.098)

Reference: EJMECH 8964

To appear in: *European Journal of Medicinal Chemistry*

Received Date: 1 August 2016

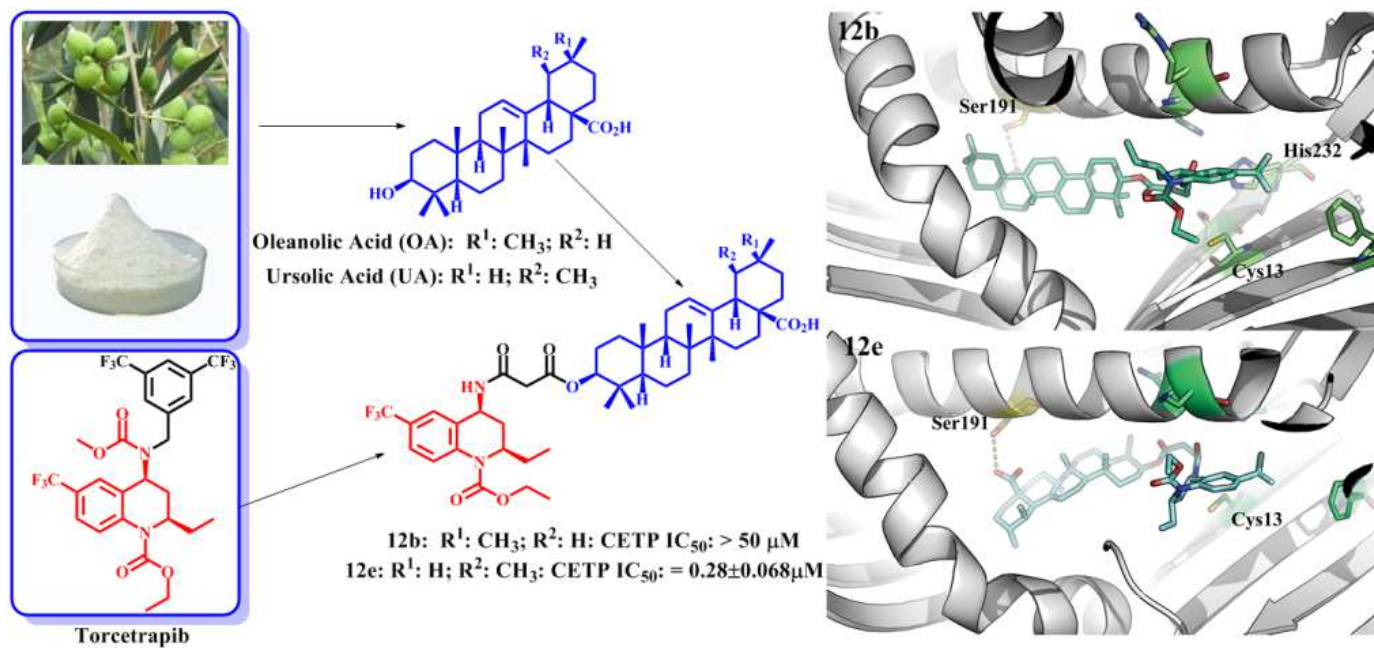
Revised Date: 28 September 2016

Accepted Date: 29 September 2016

Please cite this article as: Y. Chang, S. Zhou, E. Li, W. Zhao, Y. Ji, X. Wen, H. Sun, H. Yuan, Fragment-based discovery of novel pentacyclic triterpenoid derivatives as cholesteryl ester transfer protein inhibitors, *European Journal of Medicinal Chemistry* (2016), doi: 10.1016/j.ejmech.2016.09.098.

This is a PDF file of an unedited manuscript that has been accepted for publication. As a service to our customers we are providing this early version of the manuscript. The manuscript will undergo copyediting, typesetting, and review of the resulting proof before it is published in its final form. Please note that during the production process errors may be discovered which could affect the content, and all legal disclaimers that apply to the journal pertain.

GRAPHICAL ABSTRACT



Fragment-based Discovery of Novel Pentacyclic Triterpenoid Derivatives as Cholesteryl Ester Transfer Protein inhibitors

Yongzhi Chang, Shuxi Zhou, Enqin Li, Wenfeng Zhao, Yanpeng Ji, Xiaohan Wen*, Hongbin Sun*, Haoliang Yuan*

Jiangsu Key Laboratory of Drug Discovery for Metabolic Disease and State Key Laboratory of Natural Medicines, China Pharmaceutical University, Nanjing 210009, P.R. China

*Corresponding Author. Tel.: +86-25-83271050; Fax: +86-25-83271050; E-mail: wxagj@126.com (Xiaohan Wen); hbsun2000@yahoo.com (Hongbin Sun); yhl@cpu.edu.cn (Haoliang Yuan).

ABSTRACT

Cholesteryl Ester Transfer Protein (CETP) is an important therapeutic target for the treatment of atherosclerotic cardiovascular disease. Our molecular modeling study revealed that pentacyclic triterpenoid compounds could mimic the protein-ligand interactions of the endogenous ligand cholesteryl ester (CE) by occupying its binding site. Alignment of the docking conformations of oleanolic acid (OA), ursolic acid (UA) and the crystal conformations of known CETP inhibitor Torcetrapib in the active site proposed the applicability of fragment-based drug design (FBDD) approaches in this study. Accordingly, a series of pentacyclic triterpenoid derivatives have been designed and synthesized as novel CETP inhibitors. The most potent compound **12e** (IC₅₀: 0.28 μM) validated our strategy for molecular design. Molecular dynamics simulations illustrated that the more stable hydrogen bond interaction of the UA derivative **12e** with Ser191 and stronger hydrophobic interactions with Val198, Phe463 than those of OA derivative **12b** mainly led to their significantly different CETP inhibitory activity. These novel potent CETP inhibitors based on ursane-type scaffold should deserve further investigation.

Keywords

Pentacyclic triterpenoid; Ursolic acid; CETP inhibitor; Molecular modeling; FBDD

ABBREVIATION LIST

CETP, Cholesteryl Ester Transfer Protein;

CE, cholesteryl ester;

OA, oleanolic acid;

UA, ursolic acid;

FBDD, fragment-based drug design;

CAD, Coronary artery disease;

HDL-C, High Density Lipoprotein cholesterol;

LDL-C, Low Density Lipoprotein cholesterol;

VLDL, very low-density lipoproteins;

TG, triglyceride;

PTs, pentacyclic triterpenoids;

RMSD, root-mean-square-deviation.

1. INTRODUCTION

Coronary artery disease (CAD) derived from atherosclerosis is the leading cause of morbidity and mortality all over the world.¹⁻⁴ Large numbers of epidemiologic and clinical studies have shown an inverse relationship between High Density Lipoprotein cholesterol (HDL-C) levels and atherosclerosis, whilst a log-linear relationship between Low Density Lipoprotein cholesterol (LDL-C) and CAD events and mortality has been fully recognized.^{5,6} So for decades, the main targets of lipid-modulating therapy in an effort to prevent or treat CAD have primarily focused on either lowering LDL-C or raising HDL-C levels.^{7, 8} Currently, statin drugs (HMG-CoA reductase inhibitor), which generate impressive reductions in LDL-C, has been employed widely in the prevention and treatment of cardiovascular disease. However, limitations of statin drugs have received more attention due to some issues such as dose escalation, emergence of intolerance, adverse reactions and so on.⁹ Niacin, the most efficient HDL-C raising agent available, suffers from ubiquitous experience of flushing and indicates undesirable results in two recent clinical trials (AIM-HIGH and HPS2-THRIVE).¹⁰⁻¹² Consequently, novel lipid-modulating agents which could reasonably accommodate the balance between HDL-C and LDL-C are urgently needed to help battle emerging cardiovascular diseases.

Cholesteryl ester transfer protein (CETP), a plasma glycoprotein that mediates the transfer of cholesteryl esters (CE) from antiatherogenic apoA-containing HDL particles to proatherogenic apoB particles, primarily very low-density lipoproteins (VLDL), as for exchange, triglyceride (TG) from VLDL to HDL. The net effect of this physiological process is a decrease of serum HDL-C and increase of LDL-C.^{13, 14} Meanwhile, the discovery that a genetic deficiency involving CETP is associated with elevated levels of HDL-C and decreased LDL-C demonstrated the rationality for its pharmacological inhibition.¹⁵ Additionally, animal studies as well as clinical and epidemiologic evidence have illustrated that inhibition of CETP provides an effective strategy to raise HDL-C.¹⁶⁻¹⁸ Therefore, inhibition of CETP would be expected to produce a therapeutically beneficial plasma lipid profile and may bring clinical benefit to high risk CAD patients. Accordingly, this potential drug target has attracted the research interests of many organizations.

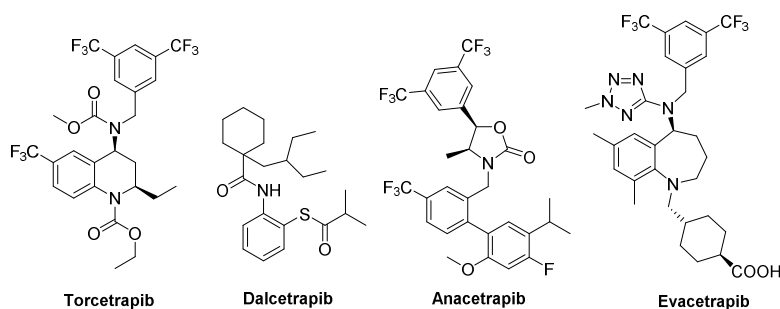


Figure 1. Representative CETP inhibitors.

To date, four CETP inhibitors have entered clinical development: Torcetrapib, Dalcetrapib, Anacetrapib, and Evacetrapib (Figure 1).¹⁹ However, only Anacetrapib developed by Merck is currently ongoing in phase III trials. In December 2006 Torcetrapib's phase III trials was terminated prematurely due to an increase in cardiovascular events and mortality.²⁰ Subsequently Roche discontinued a phase III trial of Dalcetrapib after it failed to show a clinically meaningful reduction in CV events in May 2012.²¹ In 2015 Lilly also announced to halt further research on Evacetrapib because of the lack of sufficiently clinical efficacy in a large phase III trial for patients with 'high-risk' coronary disease.²² Therefore, novel CETP inhibitors with different structural scaffolds are in urgent need to overcome the adverse effects and improve the efficacy.

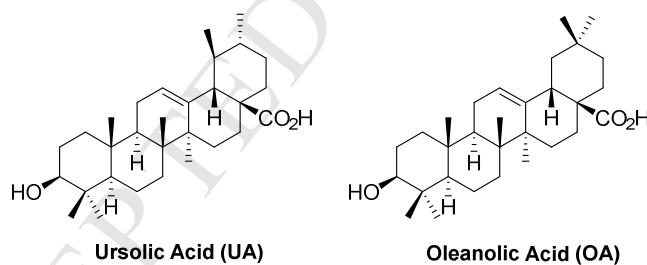


Figure 2. Natural pentacyclic triterpenes.

We supposed that it would be a feasible strategy to mimic the protein-ligand interactions of the endogenous ligand CE by occupying its binding site for the design of novel CETP inhibitors. In this regard, ursolic acid and oleanolic acid (Figure 2), which belonged to pentacyclic triterpenoids (PTs), attracted our attention due to their similar structures to cholesterol and CE. Multiple pharmacological effects of PTs have been reported, and some have been used in clinical settings.²³⁻²⁶ Molecular docking of PTs in the active site of CETP revealed their similar binding mode with the endogenous ligand, indicating the possibility of developing novel CETP

inhibitors based on these two scaffolds. Moreover, the hypolipidemic effect of UA and OA in animals has been confirmed,²⁷⁻²⁹ but the mechanism is still unclear. Alignment of the docking conformations of OA, UA and the crystal conformations of known CETP inhibitors in the active site proposed the applicability of fragment-based drug design (FBDD) approaches in this study. As PTs are noncytotoxic agents with an excellent safety profile and successful clinical utilities, introduction of active fragments from known CETP inhibitors like Torcetrapib to PTs scaffolds would provide a novel generation of CETP inhibitors. To our knowledge, this is the first study of ursane-type and oleanane-type triterpenoid compounds as CETP inhibitors.

2. RESULTS and DISCUSSION

2.1. Fragment-based Molecular Design for Novel CETP Inhibitors.

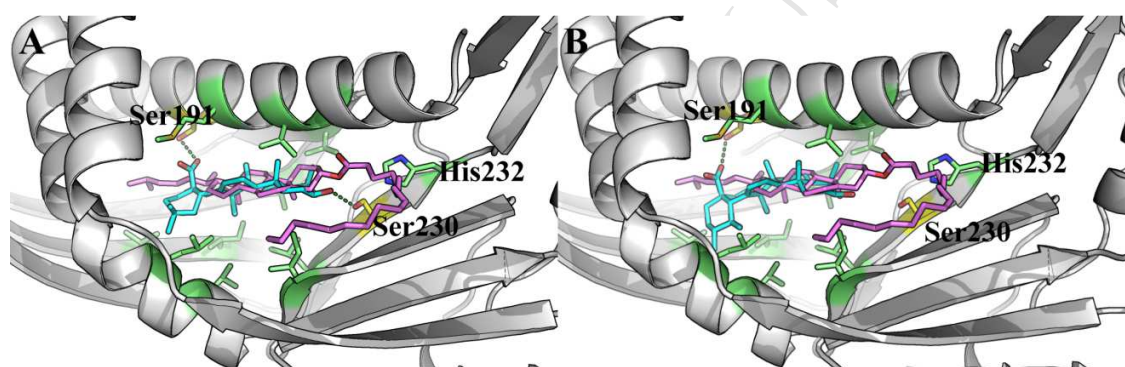


Figure 3. Alignment of docking conformation of oleanolic acid (A, blue), ursolic acid (B, blue) and the crystal conformation of CE (purple).

Fragment-based molecular design has been considered as an important methodology for lead discovery and drug design. Molecular docking of the two PTs into the active site of CETP showed that they almost occupied the binding position of the endogenous ligand CE. Besides, hydrogen bond interactions between OA and Ser191, Ser230 were observed, while one hydrogen bond between UA and Ser191 were found (Figure 3). This illustrated that these two PTs could mimic the protein-ligand interactions between the active site and CE scaffold. The crystal structure of Torcetrapib in complex with CETP was available (PDB ID: 4EWS). Alignment of the docking conformations of OA, UA and the crystal conformations of Torcetrapib in the active site showed that they were in the adjacent binding sites (Figure 4), indicating the applicability of FBDD approaches. Accordingly, we proposed the strategy for molecular design of novel CETP inhibitors by linking

the PTs scaffolds and the active fragment from Torcetrapib with the linker methylene chain (compounds **12a-12f**). Besides, the length of linker was also investigated to identify the most feasible number of methylene groups.

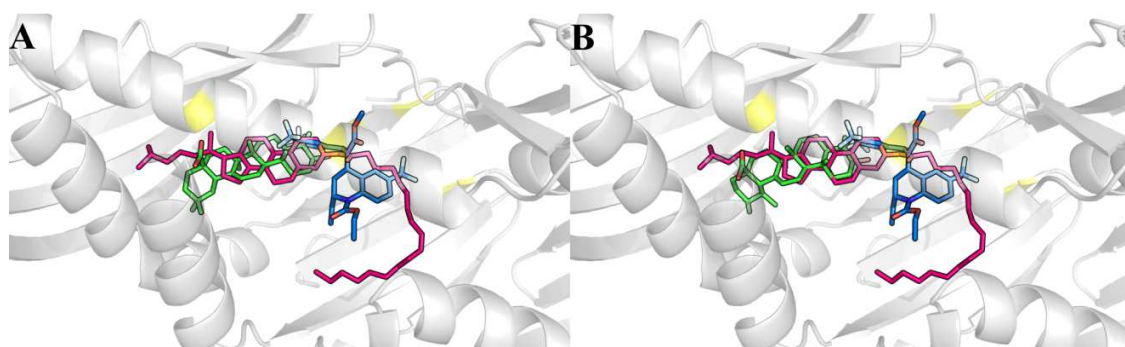


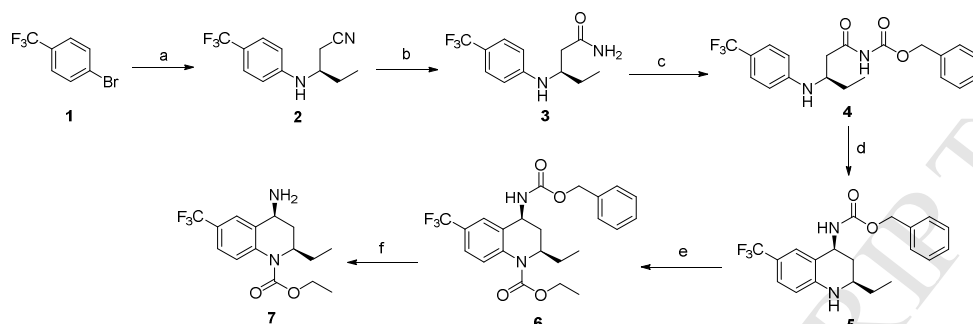
Figure 4. Alignment of docking conformation of oleanolic acid (A, green), ursolic acid (B, green), the crystal conformation of CE (red) and torcetrapib (blue).

2.2. Chemistry.

Synthesis of the target compounds **12a-f** is shown in Schemes 1-2. The tetrahydroquinoline scaffold and PTs moiety were synthesized, respectively. Overall, preparation of the tetrahydroquinoline scaffold was performed by a reported six-step procedure.^{30, 31} Preparation of substituted aniline **2** was carried out by coupling reaction of 4-bromobenzotrifluoride **1** with (*R*)-3-aminopentanenitrile in the presence of palladium acetate and cesium carbonate in toluene, then hydrolysis in sulfuric acid giving amide **3**. The key intermediate tetrahydroquinoline **5** was synthesized by treating amide **3** with benzyl chloroformate using lithium *tert*-butoxide as a base, followed by reduction of imide **4** with sodium borohydride and intramolecular cyclization. Subsequent acylation of tetrahydroquinoline with ethyl chloroformate was conducted in the presence of pyridine to afford amidate **6**, which was hydrogenated with H₂/Pd/C to generate the key intermediate **7**.

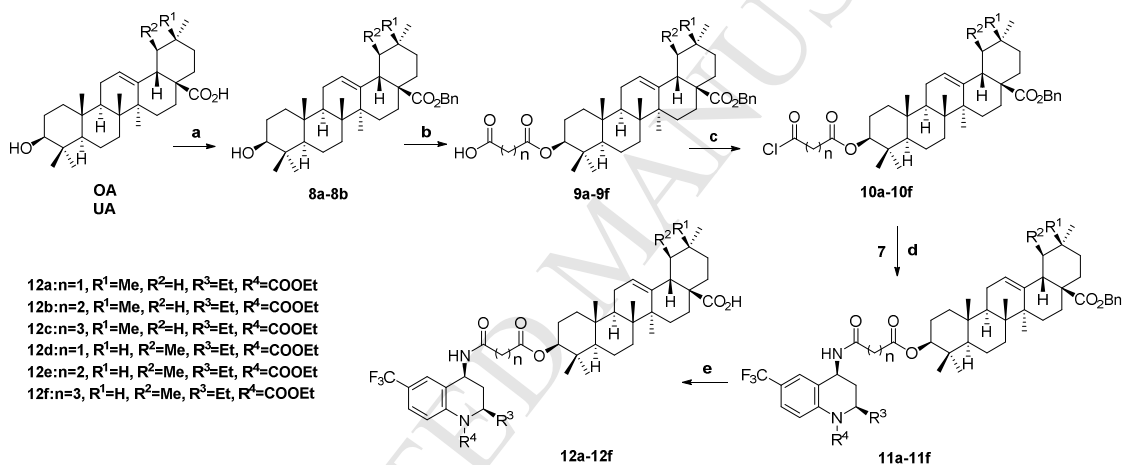
As shown in Scheme 2, condensation of OA and UA separately with benzyl chloride and potassium carbonate in DMF to provide benzyl esters **8a-b**, followed by esterification of the 3-hydroxyl group with corresponding anhydrides to afford carboxylic acids **9a-f**. The amide intermediates **11a-f** were obtained by amidation of the key intermediate **7** with corresponding acyl chlorides **10a-f**, which were prepared by treatment

of **9a-f** with thionyl chloride. Debenzoylation of **11a-f** with hydrogen over Pd/C could give target compounds **12a-f** smoothly.



Reagents and conditions: (a) (*R*)-3-aminopentanenitrile, Pd(OAc)₂, Cs₂CO₃, toluene, 80 °C; (b) 90% H₂SO₄, toluene, 100 °C; (c) benzyl chloroformate, *t*-BuOLi, isopropanol, 0 °C-rt; (d) NaBH₄, MgCl₂·6H₂O, ethanol, 0 °C-rt; (e) ethyl chloroformate, pyridine, DCM, 0 °C-rt; (f) H₂, Pd/C, HCOONH₄, MeOH, 30 °C.

Scheme 1. Synthesis of key intermediate **7**.



Reagents and conditions: (a) DMF, K₂CO₃, BnCl, 130 °C; (b) 2,2-Dimethyl-1,3-dioxane-4,6-dione, anhydrous toluene, reflux or Succinic anhydride or Glutaric anhydride, DMAP, anhydrous pyridine, reflux; (c) DCM, SOCl₂, rt; (d) DCM, Et₃N, rt; (e) MeOH, THF, H₂/Pd/C.

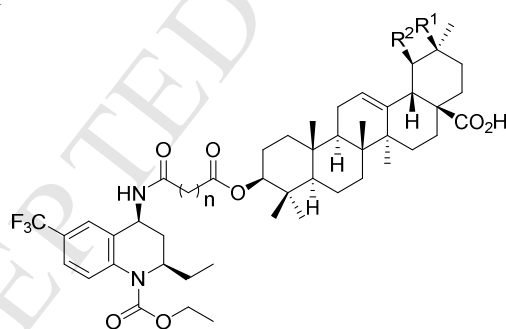
Scheme 2. Synthesis of target compounds **12a-f**.

2.3. *In Vitro* CETP Inhibition Activity.

The CETP inhibitory activities of the synthesized ursane-type and oleanane-type triterpenoid derivatives were evaluated by BODIPY-CE fluorescence assay with CETP RP Activity Kit (Catalog # RB-RPAK; Roar). Anacetrapib was used as the positive control. All compounds were tested with the commercially available CETP inhibitor drug screening kit mentioned above according to the manufacturer's protocol. The assay kit was established based on a donor molecule containing a fluorescent self-quenched neutral lipid that was transferred to an acceptor molecule in the presence of CETP (Catalog # R8899; Roar). Transfer of the fluorescent neutral lipid mediated by CETP to the acceptor molecule results in an increase in fluorescence

(ExEm = 465/535 nm). CETP inhibitors prevent the lipid transfer and consequently decrease the fluorescence intensity. From Table 1, all the ursane-type derivatives **12d-12f** exhibited potent CETP inhibition activity, but the three oleanane-type derivatives **12a-12c** showed poor activity with $IC_{50} > 50 \mu M$, indicating that the introduction of ursane-type scaffold was more suitable to fit the pocket of CETP than oleanane-type scaffold. This suggests that the difference of stereochemistry of the methyl group at carbon-19 and carbon-20 between these two types of scaffolds might play a key role for the binding of these compounds. Additionally, compound **12d** with malonyl group and compound **12f** with glutaryl group exhibited IC_{50} of $4.42 \mu M$ and $3.79 \mu M$, respectively, while the CETP inhibitory activity of compound **12e** with succinyl group was nearly 20-fold better than that of **12d** and **12f**. This indicates the significant impact of the carbon chain length on the potency. Therefore, it is concluded that the molecular conformation of compound **12e** with succinyl group is preferred to enter the relatively flat cavity of CETP in comparison with compounds **12d** and **12f**, and the length made significant effects on their CETP inhibitory activity. Moreover, the most potent compound **12e** has preliminarily confirmed our strategy for molecular design based on the PTs scaffold.

Table 1. *In vitro* CETP inhibition of compound **12a-12f**.



Compound	R ¹	R ²	n	IC ₅₀ (μM)
12a	CH ₃	H	1	> 50 ^a
12b	CH ₃	H	2	> 50
12c	CH ₃	H	3	> 50
12d	H	CH ₃	1	4.42
12e	H	CH ₃	2	0.28±0.068 ^b
12f	H	CH ₃	3	3.79
Anacetrapib				0.04±0.005 ^c

^a IC₅₀ values were determined from a single test. ^b the IC₅₀ value was expressed as the mean ± SEM of four separate tests; ^c the IC₅₀ value was expressed as the mean ± SEM of six separate tests;

2.4. Molecular Dynamics Simulations.

From Table 1, there are significant differences in CETP inhibitory activity between the ursane-type and oleanane-type triterpenoid derivatives. Compound **12e** with the best CETP inhibitory activity is the representative ursane-type compound, while **12b** is the corresponding oleanane-type congener. From their docking results in the active site of CETP, they took similar binding conformations. Hydrogen bond interactions with Ser191 for both of them were observed (Figure 5). But the conformations of the two PTs scaffolds were not in accordance with each other. Molecular dynamics simulations were carried out to investigate the detailed differences between these two compounds.

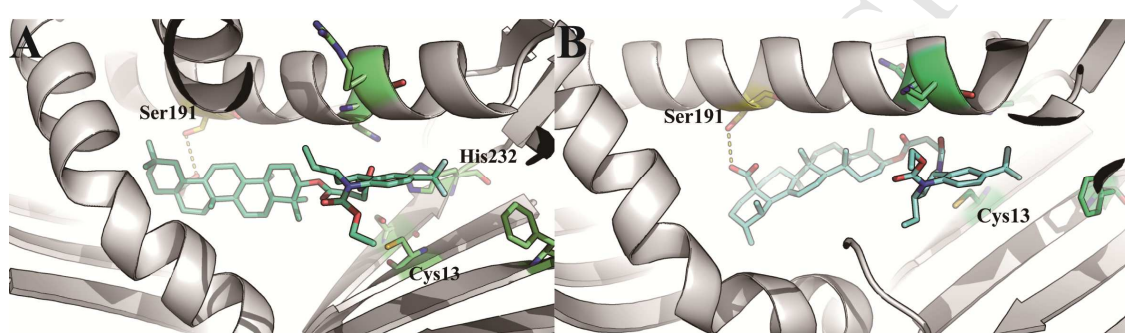


Figure 5. Docking conformation of compound **12b** (A), **12e** (B) in the active site of CETP. Yellow dash line represented hydrogen bond.

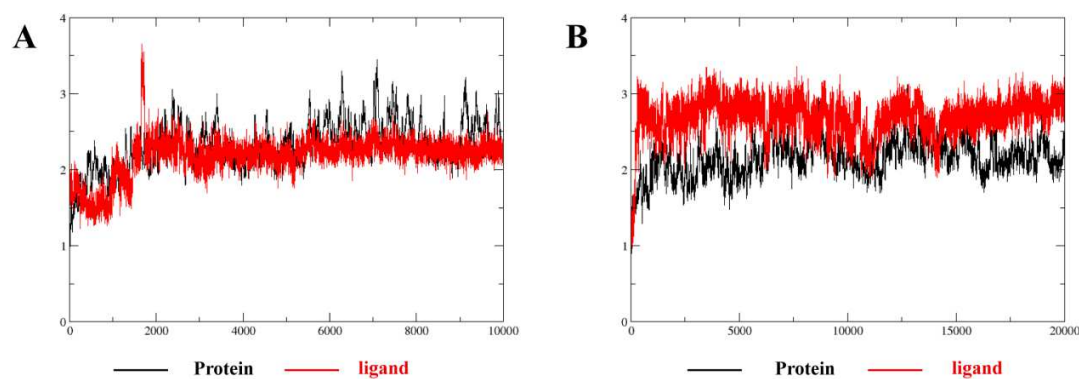


Figure 6. Changes of the backbone of protein CETP and ligands (**12b** and **12e**) in the process of molecular dynamics simulations, vertical axis represented RMSD values (Unit: Å), and horizontal axis represented time of the simulation (Unit: picosecond).

Considering the different status of the two protein-ligand systems, their simulation time was 10 and 20 ns, respectively. To explore the dynamic stability of the systems, the root-mean-square-deviation (RMSD) values using the starting structures as reference were calculated (Figure 6). For the first protein-ligand complex, the RMSD values almost converged to 2.25 Å from 2ns. For the other, the RMSD plot of protein was fluctuated in the range of 1.5-2.5 Å, and converged to 2.25 Å. The RMSD values of the ligand showed some fluctuations

around 2.75 Å. All these comparisons between the initial and dynamic conformations showed that these two protein-ligand systems were in equilibrium. Besides, the root-mean-square-fluctuation (RMSF) values of CETP in complex with compound **12b** and **12e** (Figure 7) were calculated, which showed similar tendency of the protein backbone stability. The residues in the active site kept small RMSF values, like Cys13, Ser191, Ser230 and His232, indicating they kept a stable conformation in the process of the simulations, providing a stable active site for ligand binding.

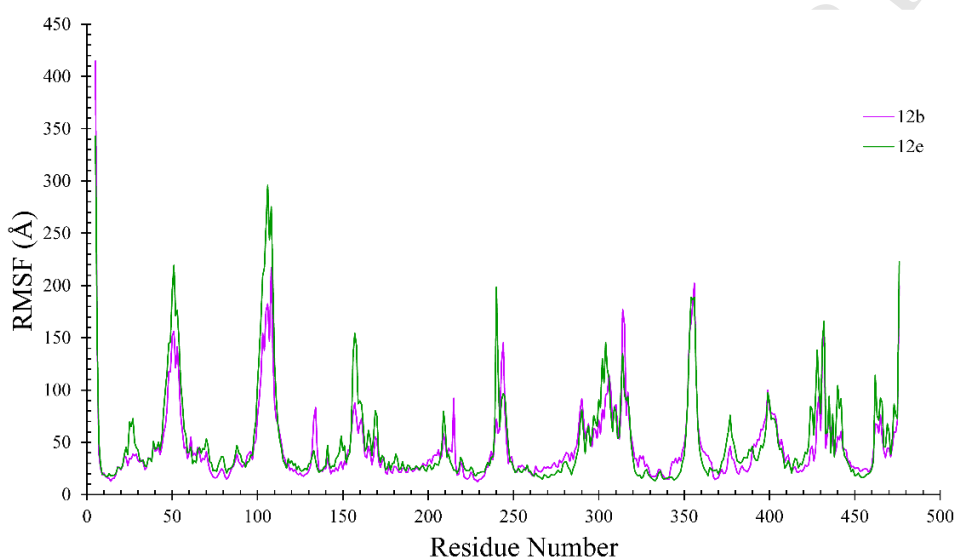


Figure 7. RMSF of CETP in complex with compound **12b** and **12e** were calculated, respectively.

The trajectory of equilibrium state was taken to analyze of hydrogen bond occupancy. It was found that compound **12e** got two hydrogen bonds with the binding site, especially the stable hydrogen bond with Ser191, occupancy of which was as high as 99.4%. For compound **12b**, two hydrogen bonds were also observed, but they were too unstable as their occupancy values were so small. Considering their similar structures except the scaffolds, the absence of this stable hydrogen bond between compound **12b** and Ser191 might contribute mainly to their significantly different CETP inhibitory activity.

Table 2. Hydrogen bond occupancy of the two compounds (**12b** and **12e**) in the selected phase of molecular dynamics simulations.

Comp.	H-Acceptor	H-Donor	Occupancy %	Distance	Angle
12b	Cys13@S	MOL@N1H49	0.93	3.382 (±0.11)	36.54 (±12.06)
	Ser191@O	MOL@O3H44	0.6	3.070 (±0.20)	57.39 (±1.90)
12e	Cys13@S	MOL@N1H49	20.2	3.361 (±0.10)	25.00 (±12.57)
	Ser191@O	MOL@O3H44	99.4	2.808 (±0.15)	24.75 (±10.34)

Binding free energy was calculated using MM/GBSA methods based on the snapshots collected from the specified equilibrium state. It could be found that their calculated binding free energy were in the same tendency with their CETP inhibitory activity. Furthermore, analysis of binding free energy profile revealed that the van-der Waals and nonpolar solvation energies were the main driving force behind the total binding free energy, which was evident from ΔE_{vdw} in case of both binding free energy calculations (Table 3). Their ΔE_{vdw} values showed they got similar hydrophobic interaction with the binding site. The strength of electronic interactions between the two inhibitors and binding site were consistent with their values of ΔE_{ele} , including the hydrogen bond interactions. The differences between their ΔE_{ele} values could be considered as the main reason for their different total binding free energy. This was in accordance with their hydrogen bond interactions with the binding site.

Table 3. Binding free energy calculated using MM/GBSA.

Contribution	12b		12e	
	Mean/(kcal/mol)	Std.	Mean/(kcal/mol)	Std.
ΔE_{ele}	-8.89	2.67	-12.46	2.30
ΔE_{vdw}	-96.00	3.60	-97.56	3.41
ΔE_{intra}	0.00	0.00	0.00	0.00
ΔE_{MM}	-104.89	4.31	-110.02	3.87
$\Delta G_{gbnonpolar}$	-13.61	0.15	-13.46	0.14
$\Delta G_{gbpolar}$	51.98	2.19	53.28	2.57
ΔG_{gbsol}	38.36	2.24	39.82	2.60
ΔG_{gbtot}	-66.52	3.50	-70.19	3.43

$$\Delta E_{MM} = \Delta E_{ele} + \Delta E_{vdw} + \Delta E_{int}; \quad \Delta G_{solvation} = \Delta G_{nonpolar} + \Delta G_{polar}; \quad \Delta G_{tot} = \Delta E_{MM} + \Delta G_{solvation}$$

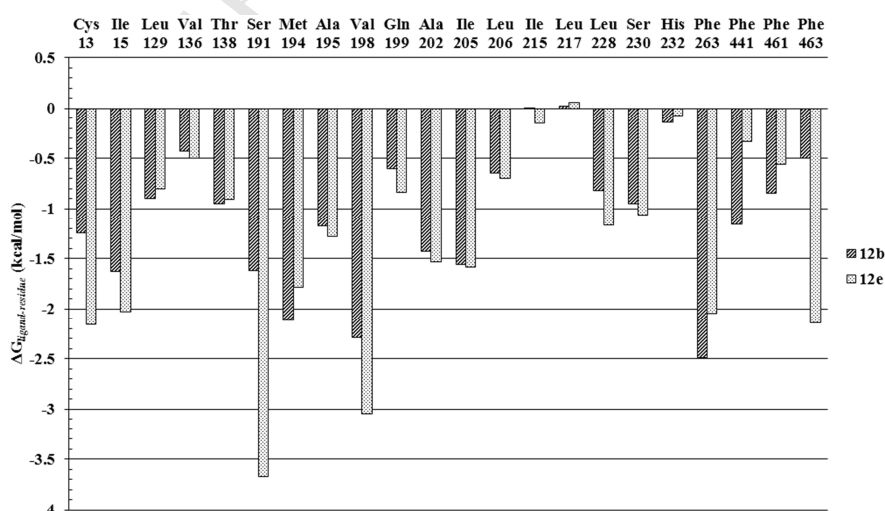


Figure 8. Comparison of per-residue energy decomposition $\Delta G_{ligand-residue}$ of CETP in complex with compound **12b** and **12e**.

Different binding conformations of compound **12b** and **12e** in the active site were resulted from the differences between their chemical structures, further resulted in different binding modes and protein-ligand interactions, and finally made different effects on their bioactivity. In order to investigate the contributions made by different protein-ligand interactions and explore the corresponding key residues making effects, per-residue binding free energy decomposition was calculated. According to the reported crystal structures, the main residues involved in the binding of CE were Cys13, Ile15, Thr138, Ser191, Met194, Val198, Gln199, Ser230 and His232,³² while the key residues involved in the binding of Torstrapib were Cys13, Ile15, Leu129, Val136, Val198, Gln199, Ala202, Ile205, Leu206, Ile215, Leu217, Leu228, Ser230, His232 and Phe263.³³ It could be found that the two sites shared some common residues, like Cys13, Val198, Gln199, Ser230 and His232, coinciding with the premise of our molecular design strategy. Table 4 summarized the comparison of energy contributions of the main residues in terms of electrostatic, vdW and solvation free energy to the binding of compound **12b** and **12e** in the active site of CETP. Most of the residues made similar energy contributions to the binding of these two compounds except several key residues. From Table 4 and Figure 8, Cys13, Ile15, Ser191, Val198 and Phe463 got better interaction with compound **12e**, while Met194, Phe263 and Phe441 got better interaction with compound **12b**. Cys13, which was in the proximity of the liner, made great contributions to the binding of compound **12e**. Although the hydrogen bond interactions with the ligands were not stable enough, the contributions in terms of electrostatic and vdW correctly reflected the different roles it has played in the binding of these two compounds. Ser191 obviously made greater contributions to the binding of compound **12e** than **12b**, mainly emphasizing on the ΔG_{ele} . This was consistent with the different stability of the hydrogen bond interactions between Ser191 and the two compounds. Val198 in the proximity of the linker got more significant vdW interaction with compound **12e** than **12b** because of their different conformations of the linker, and finally resulted in greater energy contribution to the binding of compound **12e**. The different directions of Met194 side chains and the different rotation of the PTs scaffolds led to the greater vdW interaction between Met194 and compound **12b** than **12e**. It was observed that this rotation made changes to the whole molecular conformation. Therefore, the active fragment from Torcetrapib in the two compounds

got different hydrophobic interactions with the hydrophobic pocket. This resulted in the different contributions of the related residues, such as Phe263, Phe441 and Phe463. As these two compounds got significantly different CETP inhibitory activity, it could be concluded that Cys13, Ile15, Ser191, Val198 and Phe463 were the key residues for ligand binding, especially the hydrogen bond interactions with Ser191, and hydrophobic interactions with Val198 and Phe463.

Table 4. Energy contributions of the main residues involved in the active site of CETP to the binding of inhibitors. ^a

Residues	12b				12e			
	ΔG_{vdw}	ΔG_{ele}	ΔG_{gbsol}	ΔG_{gbtot}	ΔG_{vdw}	ΔG_{ele}	ΔG_{gbsol}	ΔG_{gbtot}
Cys13	-0.96	-0.49	0.20	-1.25	-1.40	-0.67	-0.09	-2.16
Ile15	-1.49	-0.06	-0.08	-1.63	-1.85	0.05	-0.23	-2.03
Leu129	-1.22	0.13	0.19	-0.90	-1.23	0.06	0.37	-0.80
Val136	-0.96	0.04	0.49	-0.43	-1.16	0.17	0.49	-0.50
Thr138	-1.08	-0.51	0.64	-0.95	-1.15	-0.05	0.29	-0.91
Ser191	-2.07	-0.49	0.94	-1.62	-0.91	-3.12	0.37	-3.67
Met194	-2.67	0.23	0.32	-2.12	-2.16	0.32	0.06	-1.79
Ala195	-1.31	0.21	-0.08	-1.18	-1.47	0.92	-0.73	-1.28
Val198	-2.60	0.31	-0.01	-2.29	-3.21	-0.07	0.23	-3.05
Gln199	-1.02	-0.49	0.90	-0.60	-1.91	-0.83	1.91	-0.84
Ala202	-1.48	-0.16	0.21	-1.43	-1.49	-0.61	0.57	-1.53
Ile205	-1.35	-0.22	0.00	-1.56	-1.37	-0.33	0.11	-1.59
Leu206	-0.62	-0.24	0.20	-0.65	-0.64	-0.28	0.22	-0.70
Ile215	-0.07	0.03	0.05	0.01	-0.25	-0.07	0.17	-0.15
Leu217	-0.08	0.02	0.07	0.02	-0.12	0.08	0.10	0.06
Leu228	-0.98	0.09	0.07	-0.82	-1.42	-0.04	0.29	-1.17
Ser230	-0.57	-0.10	-0.28	-0.95	-0.79	-0.25	-0.02	-1.06
His232	-0.50	0.43	-0.07	-0.14	-0.84	0.00	0.76	-0.07
Phe263	-2.66	-0.06	0.24	-2.49	-2.00	0.08	-0.12	-2.05
Phe441	-1.23	-0.04	0.10	-1.16	-0.40	0.10	-0.03	-0.33
Phe461	-0.93	0.08	0.00	-0.85	-0.72	0.01	0.15	-0.56
Phe463	-0.42	-0.03	-0.06	-0.50	-1.73	-0.65	0.23	-2.14

^a All values are in kcal/mol.

3. CONCLUSIONS

In summary, a novel series of ursane-type and oleanane-type triterpenoid derivatives were designed with fragment-based method, which were then synthesized and evaluated for their CETP inhibitory activity in vitro by BODIPY-CE fluorescence assay. All the ursane-type derivatives exhibited moderate inhibitory activity. Among them, compound **12e** was identified to embody remarkable potent CETP inhibition with IC_{50} of 0.28 μ M. In addition, molecular dynamics simulation studies showed that key hydrogen bond interaction of compound **12e** with Ser191 and hydrophobic interactions with Val198 and Phe463 made great contributions to its binding. These key interactions also contributed mainly to the significant difference of CETP inhibitory

activity between compound **12b** and **12e**. Therefore, compound **12e** could be considered as a promising lead compound due to its novel scaffold, CE-mimicking binding mode and potent CETP inhibitory activity. The results of this study indicated that the novel generation of potent CETP inhibitors based on pentacyclic triterpenoid scaffold of ursolic acid deserve further investigation.

4. EXPERIMENTS

4.1 Chemistry.

Most chemicals and solvents were analytical grade and, when necessary, were purified and dried with standard methods. Melting points were taken on an XT-4 micro melting point apparatus and uncorrected. ¹H NMR spectra were recorded with a Bruker AV-300 or ACF 500 spectrometer in the indicated solvents (TMS as internal standard): the values of the chemical shifts are expressed in δ values (ppm) and the coupling constants (J) in Hz. High-resolution mass spectra were recorded using an Agilent QTOF 6520.

4.1.1 (*R*)-3-((4-(trifluoromethyl)phenyl)amino)pentanenitrile (**2**)

A mixture of 4-bromobenzotrifluoride (101 mg, 1.03 mmol), cesium carbonate (500 mg, 1.53 mmol), 2-dicyclohexylphosphino-2'-(*N,N*-dimethylamino)biphenyl (4.4 mg, 0.01 mmol), phenylboronic acid (1.86 mg, 0.015 mmol) and palladium acetate (1.8 mg, 0.008 mmol) in dry toluene (4 mL) was added to a Schlenk tube. The solution was fully degassed and charged with argon gas, then heated to 80 °C for 4 h. The reaction mixture was cooled to room temperature and filtered through Celite Pad. The solids were rinsed with toluene and the filtrate was collected and concentrated. The residue was purified by column chromatography (petroleum ether: ethyl acetate = 10:1) to afford **2** (190 mg, 76%) as a yellow oil.

4.1.2 (*R*)-3-((4-(trifluoromethyl)phenyl)amino)pentanamide (**3**)

To a solution of **2** (190 mg, 0.785 mol) in toluene (2 mL), 90% sulphuric acid (0.42 mL, 4.43 mmol) was slowly added, and the mixture stirred at 35 °C for 10 h. Then the solution was cooled to room temperature and alkalified with 20% sodium hydroxide to pH 11-12. The mixture was extracted with isopropyl ether, washed with water and brine successively, dried over anhydrous sodium sulfate, concentrated and the residue was

purified by column chromatography (petroleum ether: ethyl acetate = 2:1) to provide **3** (170 mg, 83%) as a light yellow solid.

4.1.3 (*R*)-(3-((4-(trifluoromethyl)phenyl)amino)pentanoyl) benzyl carbamate (**4**)

To a solution of **3** (390 mg, 1.5 mmol) in anhydrous isopropyl ether (6 mL) was cooled to -10 °C with ice/acetone bath. Benzyl chloroformate (305 mg, 1.8 mmol) was then added, followed by the slow addition of 1.0 M lithium tert-butoxide in THF solution (3.6 mL, 3.6 mmol) in 15 min. After stirring for another 15 min, the reaction mixture was quenched by adding 1.0 M hydrochloric acid (6 mL) and extracted with isopropyl ether. The organic phase was washed with water and brine successively, dried over anhydrous sodium sulfate, concentrated and the residue was purified by column chromatography (petroleum ether: ethyl acetate = 15:1) to provide **4** (511 mg, 86%) as a light yellow oil.

4.1.4 ((2*R*,4*S*)-2-ethyl-6-(trifluoromethyl)-1,2,3,4-tetrahydroquinolin-4-yl) benzyl carbamate (**5**)

To a solution of **4** (511 mg, 1.3 mmol) in anhydrous ethanol (12 mL) was cooled to -10 °C with ice/acetone bath, then sodium borohydride (34 mg, 0.906 mmol) was added, followed by slow addition of a solution of magnesium chloride hexahydrate (276 mg, 1.36 mmol, in 0.6 mL H₂O). The internal temperature was maintained below -5 °C during addition process. Once addition was complete, the reaction temperature was raised to 0 °C and stirred for 15 min. Then the solution was quenched with 1.0 M hydrochloric acid (6 mL) and stirred for 0.5 h at room temperature. Concentration to remove most of ethanol in vacuum and the residue was added with water and extracted with dichloromethane, then organic phase was washed with water and brine successively, dried over anhydrous sodium sulfate, concentrated and purified by column chromatography (petroleum ether : ethyl acetate = 10:1) to give **5** (442 mg, 90%) as a white solid.

4.1.5 ethyl (2*R*,4*S*)-4-(((benzyloxy)carbonyl)amino)-2-ethyl-6-(trifluoromethyl)-3,4-dihydroquinoline-1(2*H*)-carboxylate (**6**)

A mixture of **5** (150 mg, 1.89 mmol) and anhydrous pyridine (759 μ L, 9.45 mmol) in dry dichloromethane (10 mL) was slow added a solution of ethyl chloroformate (1020 mg, 9.45 mmol, in 3 mL dichloromethane) in 20 min, then the mixture was stirred at room temperature for 0.5 h and quenched with 10% sodium hydroxide

(5 ml) at 0 °C. After stirring for 15 min, the reaction mixture was extracted with dichloromethane. The combined organic layers were washed with 1.0 M hydrochloric acid, saturated aq NaHCO₃, water and brine successively, dried over anhydrous sodium sulfate, concentrated and the residue was purified by column chromatography (petroleum ether : ethyl acetate = 10:1) to provide **6** (140 mg, 76%) as a white solid.

4.1.6 ethyl (2R,4S)-4-amino-2-ethyl-6-(trifluoromethyl)-3,4-dihydroquinoline-1(2H)-carboxylate (**7**)

To a solution of **6** (215 mg, 0.5 mmol) in methane (5 mL) was added ammonium formate (80 mg, 1.25 mmol), the mixture was treated with hydrogen over 10% Pd/C (20 mg, 50% water wet) at 40 °C for 2 h. The mixture was cooled to room temperature and filtered through Celite, then the filtrate was concentrated in vacuo and the residue was purified by column chromatography (petroleum ether : ethyl acetate = 1:1) to provide **7** (113 mg, 90%) as a light yellow oil. ¹H NMR (300 MHz, CDCl₃) δ 7.74-7.71 (m, 1H), 7.57-7.44 (m, 2H), 4.46-4.39 (m, 1H), 4.34-4.14 (m, 2H), 3.88-3.79 (m, 1H), 2.59-2.45 (m, 1H), 1.71-1.62 (m, 1H), 1.53-1.39 (m, 1H), 1.33-1.24 (m, 6H), 0.86 (t, *J* = 7.4 Hz, 3H).

4.1.7 General procedure for the preparation of compounds **8a-b**

A mixture of **OA** (5 g, 0.011 mol) or **UA** (5 g, 0.011 mol), potassium carbonate (3 g, 0.022 mol) and benzyl chloride (2.5 mL, 0.022 mol) in N,N-Dimethylformamide (80 mL) was stirred at 100 °C for 5 h. Then the reaction mixture was cooled to room temperature and was poured into ice water. The mixture was extracted with ethyl acetate. The organic layer was washed with water and brine successively, dried over anhydrous sodium sulfate, concentrated in vacuo and the residue was purified by column chromatography (petroleum ether/ethyl acetate) to provide **8a-b** as a white solid.

4.1.7.1 Oleanolic acid benzyl ester (**8a**)

Compound **8a** was obtained as a white solid (5.55 g, 93%). ¹H NMR (300 MHz, CDCl₃) δ 7.33 (s, 5H), 5.28 (s, 1H), 5.09 (AB, *J* = 12.6 Hz, 1H), 5.03 (AB, *J* = 12.0 Hz, 1H), 3.23-3.18 (m, 1H), 2.90 (d, *J* = 12.0 Hz, 1H), 1.12 (s, 3H), 0.98 (s, 3H), 0.92 (s, 3H), 0.89 (s, 3H), 0.88 (s, 3H), 0.77 (s, 3H), 0.61 (s, 3H).

4.1.7.2 Ursolic acid benzyl ester (**8b**)

Compound **8b** was obtained as a white solid (5.7 g, 95%). ¹H NMR (300 MHz, CDCl₃) δ 7.33 (s, 5H), 5.23 (s, 1H), 5.10 (AB, *J* = 12.5 Hz, 1H), 4.97 (AB, *J* = 12.5 Hz, 1H), 3.23-3.18 (m, 1H), 2.27 (d, *J* = 11.3 Hz, 1H), 1.07 (s, 3H), 0.98 (s, 3H), 0.94 (s, 3H), 0.89 (s, 3H), 0.86 (s, 3H), 0.78 (s, 3H), 0.64 (s, 3H).

4.1.8 General procedure for the preparation of compounds **9a-f**

To a solution of **8a** (200 mg, 0.366 mmol) or **8b** (200 mg, 0.366 mmol) in dry toluene (3 mL) was added 2,2-Dimethyl-1,3-dioxane-4,6-dione (58 mg, 0.403 mmol). The mixture was heated to reflux for 5 h, then cooled to room temperature and concentrated in vacuo. The resulting residue was purified by column chromatography (petroleum ether/ethyl acetate) to yield **9a** and **9d** as a white solid.

To a solution of **8a** (200 mg, 0.366 mmol) or **8b** (200 mg, 0.366 mmol) in dry pyridine (5 mL) was added succinic anhydride (180 mg, 1.8 mmol) or glutaric anhydride (208 mg, 1.82 mmol) and DMAP (45 mg, 0.366 mmol). Then the mixture was heated to reflux for 10-15 h. After cooling to room temperature, the solution was poured into 1.0 M hydrochloric acid and extracted with dichloromethane. The combined organic phase was washed with water and brine successively, dried over anhydrous sodium sulfate, concentrated in vacuo and the residue was purified by column chromatography (petroleum ether/ethyl acetate) to afford **9b-9c** and **9e-9f** as a white solid.

4.1.8.1 3β-(2-carboxyacetoxy)-olean-12-en-28-oic acid benzyl ester (**9a**)

Compound **9a** was obtained as a white solid (106 mg, 46%). ¹H NMR (300 MHz, CDCl₃) δ 7.35 (s, 5H), 5.30 (s, 1H), 5.16-4.96 (m, 1H), 4.61 (t, *J* = 7.7 Hz, 1H), 3.44 (s, 2H), 2.92 (d, *J* = 11.8 Hz, 1H), 1.14 (s, 3H), 0.92 (s, 12H), 0.86 (s, 3H), 0.62 (s, 3H).

4.1.8.2 3β-((3-carboxypropanoyl)oxy)-olean-12-en-28-oic acid benzyl ester (**9b**)

Compound **9b** was obtained as a white solid (230 mg, 98%). ¹H NMR (300 MHz, CDCl₃) δ 7.33 (s, 5H), 5.29 (s, 1H), 5.14-4.92 (m, 2H), 4.51 (t, *J* = 7.6 Hz, 1H), 2.90 (d, *J* = 11.6 Hz, 1H), 2.65 (d, *J* = 6.8 Hz, 4H), 1.12 (s, 3H), 0.91 (s, 3H), 0.90 (s, 6H), 0.84 (s, 6H), 0.60 (s, 3H).

4.1.8.3 3β-((4-carboxybutanoyl)oxy)-olean-12-en-28-oic acid benzyl ester (**9c**)

Compound **9c** was obtained as a white solid (222 mg, 92%). ¹H NMR (300 MHz, CDCl₃) δ 7.33 (s, 5H), 5.28 (s, 1H), 5.14-4.96 (m, 2H), 4.57-4.43 (m, 1H), 2.90 (d, *J* = 11.1 Hz, 1H), 2.51-2.29 (m, 4H), 1.12 (s, 3H), 0.92 (s, 3H), 0.90 (s, 6H), 0.85 (s, 6H), 0.61 (s, 3H).

4.1.8.4 3β-(2-carboxyacetoxyl)-12-ursen-28-oic acid benzyl ester (**9d**)

Compound **9d** was obtained as a white solid (200 mg, 87%). ¹H NMR (300 MHz, CDCl₃) δ 7.35 (s, 5H), 5.25 (s, 1H), 5.12 (AB, *J* = 12.5 Hz, 1H), 4.99 (AB, *J* = 12.5 Hz, 1H), 4.66-4.57 (m, 1H), 3.44 (s, 2H), 2.28 (d, *J* = 11.2 Hz, 1H), 1.09 (s, 3H), 0.96 (s, 3H), 0.94 (s, 3H), 0.90 (s, 3H), 0.87 (s, 6H), 0.66 (s, 3H).

4.1.8.5 3β-((3-carboxypropanoyl)oxy)-12-ursen-28-oic acid benzyl ester (**9e**)

Compound **9e** was obtained as a white solid (220 mg, 93%). ¹H NMR (300 MHz, CDCl₃) δ 7.33 (s, 5H), 5.23 (s, 1H), 5.10 (AB, *J* = 12.5 Hz, 1H), 4.97 (AB, *J* = 12.5 Hz, 1H), 4.52 (t, *J* = 7.5 Hz, 1H), 2.68-2.61 (m, 4H), 2.26 (d, *J* = 11.1 Hz, 1H), 1.06 (s, 3H), 0.94 (s, 3H), 0.91 (s, 3H), 0.85 (s, 9H), 0.64 (s, 3H).

4.1.8.6 3β-((4-carboxybutanoyl)oxy)-12-ursen-28-oic acid benzyl ester (**9f**)

Compound **9f** was obtained as a white solid (200 mg, 83%). ¹H NMR (300 MHz, CDCl₃) δ 7.33 (s, 5H), 5.23 (s, 1H), 5.10 (AB, *J* = 12.5 Hz, 1H), 4.97 (AB, *J* = 12.5 Hz, 1H), 4.55-4.45 (m, 1H), 2.41 (m, 4H), 2.26 (d, *J* = 11.3 Hz, 1H), 1.07 (s, 3H), 0.94 (s, 3H), 0.92 (s, 3H), 0.85 (s, 9H), 0.64 (s, 3H).

4.1.9 General procedure for the preparation of compounds **11a-11f**

A mixture of acid **9a-9f** (0.16 mmol) and thionyl chloride (1 mL) in dry dichloromethane (2 mL) was stirred for 2 h at room temperature. Then dichloromethane and thionyl chloride were removed in vacuo. Yellow liquid (**10a-10f**) obtained and triethylamine (0.32 mmol) were added to a solution of intermediate **7** (0.16 mmol in 3 mL dichloromethane) at 0 °C. Then the reaction mixture was stirred at room temperature for 6 h. The solution was poured into 1.0 M hydrochloric acid and extracted with dichloromethane. The combined organic layers was washed with water and brine successively, dried over anhydrous sodium sulfate, concentrated in vacuo and the residue was purified by column chromatography (petroleum ether/ethyl acetate) to provide **11a-11f** as a white solid.

4.1.9.1 3 β -(3-(((2R,4S)-1-(ethoxycarbonyl)-2-ethyl-6-(trifluoromethyl)-1,2,3,4-tetrahydroquinolin-4-yl)amino)-3-oxopropanoyl)oxyl-olean-12-en-28-oic acid benzyl ester (11a)

Compound **11a** was obtained as a white solid. Yield: 50%. ¹H NMR (300 MHz, CDCl₃) δ 7.65-7.62 (m, 2H), 7.55-7.46 (m, 2H), 7.44 (s, 1H), 7.37-7.29 (m, 4H), 5.30 (d, J = 3.7 Hz, 1H), 5.19-5.00 (m, 3H), 4.67-4.46 (m, 2H), 4.36-4.16 (m, 3H), 3.55-3.35 (m, 2H), 2.92 (d, J = 12.9 Hz, 1H), 2.60-2.45 (m, 1H), 1.14 (s, 3H), 0.93 (s, 3H), 0.91 (s, 6H), 0.89 (s, 6H), 0.63 (s, 3H); HR-MS (ESI) m/z : calculated for C₅₅H₇₃F₃N₂O₇ [M+Na]⁺: 953.5262, found: 953.5278.

4.1.9.2 3 β -(4-(((2S,4R)-1-(ethoxycarbonyl)-2-ethyl-6-(trifluoromethyl)-1,2,3,4-tetrahydroquinolin-4-yl)amino)-4-oxobutanoyl)oxyl-olean-12-en-28-oic acid benzyl ester (11b)

Compound **11b** was obtained as a white solid. Yield: 67%. ¹H NMR (300 MHz, CDCl₃) δ 7.63-7.58 (m, 1H), 7.54-7.46 (m, 2H), 7.39-7.31 (m, 5H), 6.10 (d, J = 8.8 Hz, 1H), 5.30 (s, 1H), 5.15-4.97 (m, 3H), 4.57-4.48 (m, 2H), 4.32-4.12 (m, 3H), 2.92 (d, J = 10.2 Hz, 1H), 2.81-2.70 (m, 2H), 2.66-2.42 (m, 3H), 1.14 (s, 3H), 0.93 (s, 3H), 0.91 (s, 3H), 0.87 (s, 6H), 0.85 (s, 3H), 0.62 (s, 3H); HR-MS (ESI) m/z : calculated for C₅₆H₇₅F₃N₂O₇ [M+Na]⁺: 967.5419, found: 967.5439.

4.1.9.3 3 β -(5-(((2R,4S)-1-(ethoxycarbonyl)-2-ethyl-6-(trifluoromethyl)-1,2,3,4-tetrahydroquinolin-4-yl)amino)-5-oxopentanoyl)oxyl-olean-12-en-28-oic acid benzyl ester (11c)

Compound **11c** was obtained as a white solid. Yield: 60%. ¹H NMR (300 MHz, CDCl₃) δ 7.61-7.54 (m, 1H), 7.50-7.43 (m, 1H), 7.38 (s, 1H), 7.36-7.26 (m, 5H), 5.86 (d, J = 8.8 Hz, 1H), 5.25 (s, 1H), 5.13-4.92 (m, 3H), 4.54-4.42 (m, 2H), 4.30-4.09 (m, 3H), 2.88 (d, J = 10.8 Hz, 1H), 2.53-2.24 (m, 6H), 1.10 (s, 3H), 0.89 (s, 3H), 0.87 (s, 6H), 0.83 (s, 3H), 0.83 (s, 3H), 0.58 (s, 2H); HR-MS (ESI) m/z : calculated for C₅₇H₇₇F₃N₂O₇ [M+Na]⁺: 981.5575, found: 981.5599.

4.1.9.4 3 β -(3-(((2R,4S)-1-(ethoxycarbonyl)-2-ethyl-6-(trifluoromethyl)-1,2,3,4-tetrahydroquinolin-4-yl)amino)-3-oxopropanoyl)oxyl-12-ursen-28-oic acid benzyl ester (11d)

Compound **11d** was obtained as a white solid. Yield: 38%. ¹H NMR (300 MHz, CDCl₃) δ 7.65-7.59 (m, 2H), 7.53-7.48 (m, 1H), 7.44 (s, 1H), 7.39-7.30 (m, 5H), 5.31 (s, 1H), 5.24 (s, 1H), 5.12-4.96 (m, 3H), 4.69-4.45 (m,

2H), 4.34-4.14 (m, 3H), 3.58-3.30 (m, 2H), 2.64-2.45 (m, 1H), 2.28 (d, $J = 11.1$ Hz, 1H), 1.09 (s, 3H), 0.94 (s, 3H), 0.91 (s, 3H), 0.88 (s, 6H), 0.86 (s, 3H), 0.66 (s, 3H); HR-MS (ESI) m/z : calculated for $C_{55}H_{73}F_3N_2O_7$ $[M+Na]^+$: 953.5262, found: 953.5275.

4.1.9.5 3β -(4-(((2S,4R)-1-(ethoxycarbonyl)-2-ethyl-6-(trifluoromethyl)-1,2,3,4-tetrahydroquinolin-4-yl)amino)-4-oxobutanoyl)oxyl-12-ursen-28-oic acid benzyl ester (11e)

Compound **11e** was obtained as a white solid. Yield: 70%. 1H NMR (300 MHz, $CDCl_3$) δ 7.63-7.59 (m, 1H), 7.53-7.48 (m, 2H), 7.38-7.30 (m, 5H), 6.10 (d, $J = 8.8$ Hz, 1H), 5.30 (s, 1H), 5.15-4.96 (m, 3H), 4.59-4.45 (m, 2H), 4.32-4.14 (m, 3H), 2.82-2.73 (m, 2H), 2.65-2.58 (m, 2H), 2.56-2.45 (m, 1H), 2.28 (d, $J = 11.1$ Hz, 1H), 1.09 (s, 3H), 0.96 (s, 3H), 0.93 (s, 3H), 0.87 (s, 6H), 0.85 (s, 3H), 0.66 (s, 3H); HR-MS (ESI) m/z : calculated for $C_{56}H_{75}F_3N_2O_7$ $[M+Na]^+$: 967.5419, found: 967.5435.

4.1.9.6 3β -(5-(((2R,4S)-1-(ethoxycarbonyl)-2-ethyl-6-(trifluoromethyl)-1,2,3,4-tetrahydroquinolin-4-yl)amino)-5-oxopentanoyl)oxyl-12-ursen-28-oic acid benzyl ester (11f)

Compound **11f** was obtained as a white solid. Yield: 71%. 1H NMR (300 MHz, $CDCl_3$) δ 7.60-7.53 (m, 1H), 7.50-7.42 (m, 1H), 7.38 (s, 1H), 7.36-7.27 (m, 5H), 5.85 (d, $J = 8.8$ Hz, 1H), 5.20 (s, 1H), 5.12-4.91 (m, 3H), 4.52-4.41 (m, 2H), 4.28-4.11 (m, 3H), 2.56-2.31 (m, 6H), 2.24 (d, $J = 11.2$ Hz, 1H), 1.04 (s, 3H), 0.92 (s, 3H), 0.89 (s, 3H), 0.84 (s, 6H), 0.83 (s, 3H), 0.62 (s, 3H); HR-MS (ESI) m/z : calculated for $C_{57}H_{77}F_3N_2O_7$ $[M+Na]^+$: 981.5575, found: 981.5599.

4.1.10 General procedure for the preparation of compounds 12a-f

The ester **11a-f** (100 mg) in methane (2 ml) and tetrahydrofuran (2 ml) was reduced with hydrogen over 10% Pd/C (10 mg, 50% water wet) at room temperature for 10 h. The reaction mixture was filtered through Celite Pad, then the filtrate was concentrated in vacuo and the residue was purified by column chromatography (petroleum ether/ethyl acetate) to provide target compounds **12a-f** as a white solid.

4.1.10.1 3β -(3-(((2R,4S)-1-(ethoxycarbonyl)-2-ethyl-6-(trifluoromethyl)-1,2,3,4-tetrahydroquinolin-4-yl)amino)-3-oxopropanoyl)oxyl-olean-12-en-28-oic acid (12a)

Compound **12a** was obtained as a white solid. Yield: 61%. mp. 140-142°C; ¹H NMR (300 MHz, CDCl₃) δ 7.67-7.64 (m, 1H), 7.61 (s, 1H), 7.51-7.49 (m, 1H), 7.43 (s, 1H), 5.28 (s, 1H), 5.13-5.11 (m, 1H), 4.62-4.59 (m, 1H), 4.53-4.49 (m, 1H), 4.27-4.22 (m, 2H), 3.53-3.40 (m, 2H), 2.84-2.80 (m, 1H), 2.54-2.48 (s, 1H), 1.14 (s, 3H), 0.95 (s, 3H), 0.93 (s, 3H), 0.91 (s, 3H), 0.91 (s, 3H), 0.88 (s, 3H); ¹³C NMR (75 MHz, CDCl₃) δ 183.45, 169.59, 164.99, 154.37, 143.66, 139.51, 133.21, 126.14, 124.24, 122.31, 121.10, 83.06, 62.21, 55.22, 53.27, 47.51, 46.46, 45.83, 44.57, 41.56, 41.12, 40.92, 39.25, 37.99, 37.74, 37.08, 36.91, 33.74, 32.98, 32.47, 32.37, 30.60, 29.62, 28.40, 27.97, 27.89, 27.61, 25.84, 23.77, 23.51, 23.33, 22.85, 18.11, 17.02, 16.57, 15.29, 14.35, 9.90, 7.83; HR-MS (ESI) *m/z*: calculated for C₄₈H₆₇F₃N₂O₇ [M+Na]⁺ 863.4793, found 863.4766.

4.1.10.2 3β-(4-(((2S,4R)-1-(ethoxycarbonyl)-2-ethyl-6-(trifluoromethyl)-1,2,3,4-tetrahydroquinolin-4-yl)amino)-4-oxobutanoyl)oxyl-olean-12-en-28-oic acid (12b)

Compound **12b** was obtained as a white solid. Yield: 60%. m.p. 129-130°C; ¹H NMR (300 MHz, CDCl₃) δ 7.59-7.56 (m, 1H), 7.49-7.48 (m, 2H), 6.17 (d, *J* = 8.7 Hz, 1H), 5.27 (s, 1H), 5.08-5.01 (m, 1H), 4.56-4.43 (m, 2H), 4.29-4.16 (m, 2H), 2.84-2.45 (m, 6H), 1.14 (s, 3H), 0.93 (s, 3H), 0.90 (s, 3H), 0.88 (s, 3H), 0.86 (s, 3H), 0.84 (s, 3H), 0.75 (s, 3H); ¹³C NMR (75 MHz, CDCl₃) δ 183.38, 173.11, 172.20, 171.51, 168.43, 154.42, 143.66, 136.99, 133.85, 126.15, 124.23, 122.47, 121.02, 81.80, 62.20, 55.26, 53.35, 47.54, 46.53, 45.87, 44.77, 41.59, 40.98, 39.29, 38.05, 37.71, 37.43, 36.96, 33.80, 33.03, 32.54, 32.44, 31.47, 30.65, 29.96, 29.68, 28.14, 27.96, 27.67, 25.84, 23.56, 23.40, 22.92, 18.15, 17.10, 16.66, 15.35, 14.41, 9.89; HR-MS (ESI) *m/z*: calculated for C₄₉H₆₉F₃N₂O₇ [M+Na]⁺ 877.4949, found 877.4960.

4.1.10.3 3β-(5-(((2R,4S)-1-(ethoxycarbonyl)-2-ethyl-6-(trifluoromethyl)-1,2,3,4-tetrahydroquinolin-4-yl)amino)-5-oxopentanoyl)oxyl-olean-12-en-28-oic acid (12c)

Compound **12c** was obtained as a white solid. Yield: 74%. mp.: 133-135°C; ¹H NMR (300 MHz, CDCl₃) δ 7.60-7.58 (m, 1H), 7.49-7.46 (m, 1H), 7.40 (s, 1H), 5.98 (d, *J*=6.0 Hz, 1H), 5.26 (s, 1H), 5.11-5.03 (m, 1H), 4.54-4.46 (m, 2H), 4.28-4.16 (m, 2H), 2.84-2.78 (m, 1H), 2.53-2.30 (m, 6H), 1.12 (s, 3H), 0.93 (s, 3H), 0.92 (s, 3H), 0.89 (s, 3H), 0.87 (s, 3H), 0.86 (s, 3H), 0.74 (s, 3H); ¹³C NMR (75 MHz, CDCl₃) δ 183.47, 173.09, 171.99, 154.40, 143.64, 139.60, 133.68, 126.22, 124.26, 122.47, 120.91, 114.61, 81.23, 62.23, 55.29, 53.33,

47.55, 46.51, 45.86, 44.62, 41.58, 40.95, 39.28, 38.05, 37.72, 37.37, 36.97, 35.60, 33.78, 33.67, 33.03, 32.53, 30.64, 29.67, 28.10, 28.06, 27.66, 25.87, 23.55, 23.38, 22.89, 21.22, 18.16, 17.13, 16.67, 15.34, 14.39, 9.90; HR-MS (ESI) m/z : calculated for $C_{50}H_{71}F_3N_2O_7$ $[M+Na]^+$ 891.5106, found 891.5120.

4.1.10.4 3β -(3-(((2R,4S)-1-(ethoxycarbonyl)-2-ethyl-6-(trifluoromethyl)-1,2,3,4-tetrahydroquinolin-4-yl)amino)-3-oxopropanoyl)oxyl-12-ursen-28-oic acid (12d)

Compound **12d** was obtained as a white solid. Yield: 59%. mp.: 152-154°C; 1H NMR (300 MHz, $CDCl_3$) δ 7.68-7.64 (m, 1H), 7.61 (s, 1H), 7.52-7.49 (m, 1H), 7.44 (s, 1H), 5.25 (s, 1H), 5.17-5.09 (m, 1H), 4.65-4.60 (m, 1H), 4.54-4.47 (m, 1H), 4.31-4.19 (m, 2H), 3.54-3.41 (m, 2H), 2.58-2.49 (m, 1H), 2.22-2.18 (m, 1H), 1.09 (s, 3H), 0.97 (s, 3H), 0.91 (s, 3H), 0.88 (s, 6H), 0.86 (s, 3H), 0.79 (s, 3H); ^{13}C NMR (75 MHz, $CDCl_3$) δ 183.23, 169.59, 164.98, 154.37, 137.97, 133.21, 126.14, 125.53, 124.24, 121.06, 83.08, 62.21, 55.23, 53.27, 52.50, 47.89, 47.43, 44.56, 41.91, 41.10, 39.47, 38.97, 38.77, 38.18, 37.74, 37.08, 36.84, 36.63, 32.77, 30.54, 28.40, 28.02, 27.89, 24.01, 23.76, 23.52, 23.23, 21.09, 18.10, 16.92, 16.62, 15.44, 14.35, 9.91, 7.83; HR-MS (ESI) m/z : calculated for $C_{48}H_{67}F_3N_2O_7$ $[M+Na]^+$ 863.4793, found 863.4795.

4.1.10.5 3β -(4-(((2S,4R)-1-(ethoxycarbonyl)-2-ethyl-6-(trifluoromethyl)-1,2,3,4-tetrahydroquinolin-4-yl)amino)-4-oxobutanoyl)oxyl-12-ursen-28-oic acid (12e)

Compound **12e** was obtained as a white solid. Yield: 73%. mp.: 138-140°C; 1H NMR (300 MHz, $CDCl_3$) δ 7.60-7.58 (m, 1H), 7.50-7.48 (m, 2H), 6.23 (d, $J=9.0$ Hz, 1H), 5.24 (s, 1H), 5.06-5.04 (m, 1H), 4.56-4.46 (m, 2H), 4.29-4.13 (m, 2H), 2.76-2.60 (m, 4H), 2.54-2.45 (m, 1H), 2.20-2.17 (m, 1H), 1.08 (s, 3H), 0.95 (s, 3H), 0.88 (s, 3H), 0.86 (s, 6H), 0.84 (s, 3H), 0.77 (s, 3H); ^{13}C NMR (75 MHz, $CDCl_3$) δ 183.06, 173.10, 171.50, 154.42, 139.55, 138.86, 138.02, 135.36, 133.86, 126.15, 125.66, 124.23, 124.18, 121.07, 81.79, 62.20, 55.26, 53.36, 52.56, 47.93, 47.45, 44.76, 41.92, 39.50, 39.02, 38.82, 38.24, 37.71, 37.43, 36.88, 36.71, 32.83, 31.45, 30.60, 29.95, 29.68, 28.14, 27.99, 24.07, 23.53, 23.28, 21.15, 18.13, 17.06, 16.99, 16.71, 15.49, 14.41, 9.90; HR-MS (ESI) m/z : calculated for $C_{49}H_{69}F_3N_2O_7$ $[M+Na]^+$ 877.4949, found 877.4953.

4.1.10.6 3β -(5-(((2R,4S)-1-(ethoxycarbonyl)-2-ethyl-6-(trifluoromethyl)-1,2,3,4-tetrahydroquinolin-4-yl)amino)-5-oxopentanoyl)oxyl-12-ursen-28-oic acid (12f)

Compound **12f** was obtained as a white solid. Yield: 77%. mp. 153-155°C; ^1H NMR (300 MHz, CDCl_3) δ 7.61-7.58 (m, 1H), 7.50-7.47 (m, 1H), 7.41 (s, 1H), 6.02 (d, $J=9.0$ Hz, 1H), 5.23 (s, 1H), 5.11-5.04 (m, 1H), 4.54-4.47 (m, 2H), 4.28-4.16 (m, 2H), 2.50-2.37 (m, 6H), 2.19-2.16 (m, 1H), 1.07 (s, 3H), 0.94 (s, 6H), 0.86 (s, 3H), 0.85 (s, 6H), 0.76 (s, 3H); ^{13}C NMR (75 MHz, CDCl_3) δ 183.30, 173.10, 172.02, 154.41, 153.48, 137.99, 134.28, 133.69, 126.22, 125.65, 124.21, 120.87, 81.25, 62.24, 55.29, 53.34, 52.53, 47.93, 47.46, 44.63, 41.91, 39.50, 39.01, 38.82, 38.24, 37.72, 37.37, 36.90, 36.71, 35.61, 33.68, 32.82, 30.59, 29.67, 28.10, 27.98, 24.04, 23.56, 23.27, 21.22, 21.14, 18.14, 17.07, 16.99, 16.72, 15.49, 14.39, 9.90; HR-MS (ESI) m/z : calculated for $\text{C}_{50}\text{H}_{71}\text{F}_3\text{N}_2\text{O}_7$ $[\text{M}+\text{Na}]^+$ 891.5106, found 891.5120.

4.2. CETP inhibitory assay.

The CETP inhibitory bioactivities of the synthesized compounds were determined by using a standard fluorescent-CE transfer assay. The assay procedure can be described briefly as follows. Testing compounds were totally dissolved in 100% DMSO and stored at nitrogen cabinet. Reconstitute the 80 $\mu\text{g}/\text{ml}$ rCETP in total protein with assay buffer and dilute the stocking compounds (10mM) with DMSO for 8 points titration (1:5 serial dilutions) in 96-well dilution plate. A solution that contains no rCETP was as background and that contains rCETP but no testing compounds as the positive control. Donor molecule (4 μL), acceptor molecule (4 μL) and testing compound (1 μL) with rCETP (30 ng) were mixed in assay buffer (200 μL). After incubation at 37 °C for 3 h, fluorescence intensity was read in a fluorimeter (Flex Station III) and the inhibition ratio was also calculated.

4.3. Molecular docking and molecular dynamics simulation.

All molecular docking procedures were completed in Schrödinger 2009. The crystal structure of CETP in complex with CE (PDB ID: 2OBD) was applied in molecular modeling. The protein in the crystal structures was prepared using the *Protein Preparation Wizard* workflow. The generated receptor grid was centered on the endogenous ligand CE in the crystal structure, which was defined as the ligand-binding site search region. The compounds to be docked was confirmed by an enclosing box that was similar in size to the crystal ligand. The compounds were prepared with *LigPrep* and docked into the binding site using *Glide* extra precision (XP)

mode. Default settings were used for all the other parameters. The best pose was determined by Glide score and interactions between the compounds and CETP.

Molecular dynamics simulations were performed using the AMBER 14 software package with the ff99SB force field³⁴ to simulate CETP in complex with compounds **12b** and **12e** and calculate their binding free energy. The co-complex structures were obtained by molecular docking. The ligands were firstly fully minimized by the AM1 method and electrostatic potentials computed at the HF/6-31G* level in the Gaussian 09 program. The RESP fitting technique in AMBER 14 was used to determine the partial charges. The force-field parameters for the ligand were generated with the general AMBER force field (GAFF) by the Antechamber program.³⁵ Hydrogen atoms were assigned using the LEaP module, which sets ionisable residues to their default protonation states at a neutral pH value. Each complex was immersed in a cubic box of TIP3P water model with a 10 Å minimum solute-wall distance.³⁶ A total of fifteen Na⁺ ions were added to neutralize each protein-ligand complex system. Energy was minimized in the solvated system employing 1000 steps of the steepest descent algorithm and 2000 steps of the conjugate gradient algorithm with a nonbonded cutoff of 10Å. The protocol for molecular dynamics simulation consisting of gradual heating, density equilibration, equilibration and production procedures in an isothermal isobaric ensemble (*NPT*, *P* = 1 atm and *T* = 298K) MD. The system was gradually heated from 0 to 298K in 50ps, followed by density equilibration at 298K for 500ps, and then constant equilibration at 298K for 500ps. Then each protein-ligand complex system underwent a process of equilibration procedure until the system achieved a continuous stable status, i.e. production stage. The time step was set to 2fs while the snapshots were taken every 10 ps to record the conformation trajectory during production MD. The nonbonded interactions were treated with a 10Å cutoff.³⁷ SHAKE algorithm³⁸ was applied to constrain all bonds involving hydrogen atoms to their equilibrium length. The conformations of different systems were collected every 50ps after the system achieved their equilibrium status. The collected snapshots were used for structural and energetic analysis of each complex system.

Binding free energy calculations were also performed to investigate the differences of binding affinity between different ligands and the binding pocket. The method of and MM/GBSA³⁹ is used for investigating the

energetic contribution of protein-ligand binding affinities. For different protein-ligand systems, the process of converged status was used for the binding free energy calculation. The solute and solvent dielectric constants were set as 1.0 and 80.0, respectively. The binding free energy of different ligands to the protein was calculated as follows:

$$\Delta G_{binding} = G_{complex} - [G_{protein} + G_{ligand}]$$

For different protein-ligand systems, the process for binding free energy calculations were also applied for hydrogen bond occupancy calculations. The hydrogen bond distance was set as 3.5Å and angle was 120.0°. Other parameters were kept default.

Binding free energy was decomposed to each residue to identify the key residues contributed greatly to the binding process of inhibitors. The interactions between inhibitor and each residue were computed using MM/GBSA decomposition procedure in Amber 14. Four components were included in the binding interaction of each inhibitor-residue pair: van der Waals contribution (ΔG_{vdW}), electrostatic contribution (ΔG_{ele}) and solvation contribution (ΔG_{bsol}).

ACKNOWLEDGEMENTS

The authors are grateful to National Natural Science Foundation of China (81373303, 81473080, 81573299, and 21502230), Promotive Research Fund for Excellent Young and Middle-aged Scientists of Jiangsu Province (BS2010YY073), Jiangsu Provincial Natural Science Foundation (ZR2012HM036) and the scientific research fund for new teacher of China Pharmaceutical University (3014070086) for financial support.

Appendix A. Supplementary data

Supplementary data related to this article can be found at

REFERENCES

- [1] Z. Lu, J. B. Napolitano, A. Theberge, A. Ali, M. L. Hammond, E. Tan, X. Tong, S. S. Xu, M. J. Latham, L. B. Peterson, M. S. Anderson, S. S. Eveland, Q. Guo, S. A. Hyland, D. P. Milot, Y. Chen, C. P. Sparrow, S. D. Wright, P. J. Sinclair, Design of a novel class of biphenyl CETP inhibitors, *Bioorg. Med. Chem. Lett.* 20 (2010) 7469-72.
- [2] E. S. Ford, S. Capewell, Coronary heart disease mortality among young adults in the U.S. from 1980 through 2002: concealed leveling of mortality rates, *J. Am. Coll. Cardiol.* 50 (2007) 2128-32.
- [3] R. Kones, U. Rumana, Current Treatment of Dyslipidemia: Evolving Roles of Non-Statins and Newer Drugs, *Drugs* 75 (2015) 1201-28.
- [4] R. Kones, U. Rumana, Current Treatment of Dyslipidemia: A New Paradigm for Statin Drug Use and the Need for Additional Therapies, *Drugs* 75 (2015) 1187-99.
- [5] F. Barzi, A. Patel, M. Woodward, C. M. Lawes, T. Ohkubo, D. Gu, T. H. Lam, H. Ueshima, C. Asia Pacific Cohort Studies, A comparison of lipid variables as predictors of cardiovascular disease in the Asia Pacific region, *Ann. Epidemiol.* 15 (2005) 405-13.
- [6] S. M. Grundy, J. I. Cleeman, C. N. Merz, H. B. Brewer, Jr., L. T. Clark, D. B. Hunninghake, R. C. Pasternak, S. C. Smith, Jr., N. J. Stone, L. National Heart, I. Blood, F. American College of Cardiology, A. American Heart, Implications of recent clinical trials for the National Cholesterol Education Program Adult Treatment Panel III guidelines, *Circulation* 110 (2004) 227-39.
- [7] D. J. Gordon, J. L. Probstfield, R. J. Garrison, J. D. Neaton, W. P. Castelli, J. D. Knoke, D. R. Jacobs, Jr., S. Bangdiwala, H. A. Tyroler, High-density lipoprotein cholesterol and cardiovascular disease. Four prospective American studies, *Circulation* 79 (1989) 8-15.
- [8] B. Paigen, B. Y. Ishida, J. Verstuyft, R. B. Winters, D. Albee, Atherosclerosis susceptibility differences among progenitors of recombinant inbred strains of mice, *Arteriosclerosis* 10 (1990) 316-23.
- [9] M. D. Carroll, D. A. Lacher, P. D. Sorlie, J. I. Cleeman, D. J. Gordon, M. Wolz, S. M. Grundy, C. L. Johnson, Trends in serum lipids and lipoproteins of adults, 1960-2002, *JAMA* 294 (2005) 1773-81.
- [10] M. C. Brouwers, C. D. Stehouwer, Niacin in cardiovascular patients receiving statins, *N. Engl. J. Med.* 366 (2012) 1255; author reply 1255-6.
- [11] H. T. C. Group, M. J. Landray, R. Haynes, J. C. Hopewell, S. Parish, T. Aung, J. Tomson, K. Wallendszus, M. Craig, L. Jiang, R. Collins, J. Armitage, Effects of extended-release niacin with laropiprant in high-risk patients, *N. Engl. J. Med.* 371 (2014) 203-12.
- [12] T. J. Anderson, W. E. Boden, P. Desvigne-Nickens, J. L. Fleg, M. L. Kashyap, R. McBride, J. L. Probstfield, A.-H. Investigators, Safety profile of extended-release niacin in the AIM-HIGH trial, *N. Engl. J. Med.* 371 (2014) 288-90.
- [13] J. A. Hunt, Z. Lu, Cholesteryl ester transfer protein (CETP) inhibitors, *Curr. Top. Med. Chem.* 9 (2009) 419-27.
- [14] S. J. Nicholls, E. M. Tuzcu, I. Sipahi, A. W. Grasso, P. Schoenhagen, T. Hu, K. Wolski, T. Crowe, M. Y. Desai, S. L. Hazen, S. R. Kapadia, S. E. Nissen, Statins, high-density lipoprotein cholesterol, and regression of coronary atherosclerosis, *JAMA* 297 (2007) 499-508.
- [15] F. Matsuura, N. Wang, W. Chen, X. C. Jiang, A. R. Tall, HDL from CETP-deficient subjects shows enhanced ability to promote cholesterol efflux from macrophages in an apoE- and ABCG1-dependent pathway, *J. Clin. Invest.* 116 (2006) 1435-42.
- [16] Y. C. Ha, P. J. Barter, Differences in plasma cholesteryl ester transfer activity in sixteen vertebrate species, *Comp. Biochem. Physiol. B Biochem. Mol. Biol.* 71 (1982) 265-9.
- [17] K. R. Marotti, C. K. Castle, T. P. Boyle, A. H. Lin, R. W. Murray, G. W. Melchior, Severe atherosclerosis in transgenic mice expressing simian cholesteryl ester transfer protein, *Nature* 364 (1993) 73-5.
- [18] J. D. Curb, R. D. Abbott, B. L. Rodriguez, K. Masaki, R. Chen, D. S. Sharp, A. R. Tall, A prospective study of HDL-C and cholesteryl ester transfer protein gene mutations and the risk of coronary heart disease in the elderly, *J. Lipid Res.* 45 (2004) 948-53.
- [19] B. A. Kingwell, M. J. Chapman, A. Kontush, N. E. Miller, HDL-targeted therapies: progress, failures and future, *Nat. Rev. Drug Discov.* 13 (2014) 445-64.
- [20] P. J. Barter, M. Caulfield, M. Eriksson, S. M. Grundy, J. J. Kastelein, M. Komajda, J. Lopez-Sendon, L. Mosca, J. C. Tardif, D. D. Waters, C. L. Shear, J. H. Revkin, K. A. Buhr, M. R. Fisher, A. R. Tall, B. Brewer, I. Investigators, Effects of torcetrapib in patients at high risk for coronary events, *N. Engl. J. Med.* 357 (2007) 2109-22.
- [21] D. S. Robinson, H. H. Kariyawasam, Mepolizumab for eosinophilic severe asthma: recent studies, *Expert. Opin. Biol. Ther.* 15 (2015) 909-14.
- [22] S. Stiles, Lilly Pulls Plug on Its CETP Inhibitor Evacetrapib, *Medscape* (October 12, 2015).
- [23] S. Jager, H. Trojan, T. Kopp, M. N. Laszczyk, A. Scheffler, Pentacyclic triterpene distribution in various plants - rich sources for a new group of multi-potent plant extracts, *Molecules* 14 (2009) 2016-31.
- [24] Y. Muto, M. Ninomiya, H. Fujiki, Present status of research on cancer chemoprevention in Japan, *Jpn. J. Clin. Oncol.* 20 (1990) 219-24.
- [25] P. Dzubak, M. Hajdich, D. Vydra, A. Hustova, M. Kvasnica, D. Biedermann, L. Markova, M. Urban, J. Sarek, Pharmacological activities of natural triterpenoids and their therapeutic implications, *Nat. Prod. Rep.* 23 (2006) 394-411.
- [26] H. Sheng, H. Sun, Synthesis, biology and clinical significance of pentacyclic triterpenes: a multi-target approach to prevention and treatment of metabolic and vascular diseases, *Nat. Prod. Rep.* 28 (2011) 543-93.

- [27] L. O. Somova, A. Nadar, P. Rammanan, F. O. Shode, Cardiovascular, antihyperlipidemic and antioxidant effects of oleanolic and ursolic acids in experimental hypertension, *Phytomedicine* 10 (2003) 115-21.
- [28] K. Yunoki, G. Sasaki, Y. Tokuji, M. Kinoshita, A. Naito, K. Aida, M. Ohnishi, Effect of dietary wine pomace extract and oleanolic acid on plasma lipids in rats fed high-fat diet and its DNA microarray analysis, *J. Agric. Food Chem.* 56 (2008) 12052-8.
- [29] Y. Feleke, D. Fekade, Y. Mezegebu, Prevalence of highly active antiretroviral therapy associated metabolic abnormalities and lipodystrophy in HIV infected patients, *Ethiop. Med. J.* 50 (2012) 221-30.
- [30] D. B. Damon, R. W. Dugger, S. E. Hubbs, J. M. Scott, R. W. Scott, Asymmetric Synthesis of the Cholesteryl Ester Transfer Protein Inhibitor Torcetrapib, *Org. Process Res. Dev.* 10 (2006) 472-480.
- [31] D. B. Damon, R. W. Dugger, G. Magnus-Aryitey, R. B. Ruggeri, R. T. Wester, M. Tu, Y. Abramov, Synthesis of the CETP Inhibitor Torcetrapib: The Resolution Route and Origin of Stereoselectivity in the Iminium Ion Cyclization, *Org. Process Res. Dev.* 10 (2006) 464-471.
- [32] X. Qiu, A. Mistry, M. J. Ammirati, B. A. Chrnyk, R. W. Clark, Y. Cong, J. S. Culp, D. E. Danley, T. B. Freeman, K. F. Geoghegan, M. C. Griffor, S. J. Hawrylik, C. M. Hayward, P. Hensley, L. R. Hoth, G. A. Karam, M. E. Lira, D. B. Lloyd, K. M. McGrath, K. J. Stutzman-Engwall, A. K. Subashi, T. A. Subashi, J. F. Thompson, I. K. Wang, H. Zhao, A. P. Seddon, Crystal structure of cholesteryl ester transfer protein reveals a long tunnel and four bound lipid molecules, *Nat. Struct. Mol. Biol.* 14 (2007) 106-13.
- [33] S. Liu, A. Mistry, J. M. Reynolds, D. B. Lloyd, M. C. Griffor, D. A. Perry, R. B. Ruggeri, R. W. Clark, X. Qiu, Crystal structures of cholesteryl ester transfer protein in complex with inhibitors, *J. Biol. Chem.* 287 (2012) 37321-9.
- [34] Y. Duan, C. Wu, S. Chowdhury, M. C. Lee, G. Xiong, W. Zhang, R. Yang, P. Cieplak, R. Luo, T. Lee, J. Caldwell, J. Wang, P. Kollman, A point-charge force field for molecular mechanics simulations of proteins based on condensed-phase quantum mechanical calculations, *J. Comput. Chem.* 24 (2003) 1999-2012.
- [35] J. Wang, W. Wang, P. A. Kollman, D. A. Case, Automatic atom type and bond type perception in molecular mechanical calculations, *J. Mol. Graph. Model.* 25 (2006) 247-60.
- [36] W. L. C. Jorgensen, J.; Madura, J. D.; Impey, R. W.; M. L. Klein, Comparison of simple potential functions for simulating liquid water., *J. Chem. Phys.* 79 (1983) 926-935.
- [37] T. Y. Darden, D.; Pedersen, L. Particle mesh Ewald., Particle mesh Ewald: An N-log(N) method for Ewald sums in large systems, *J. Chem. Phys.* 98 (1993) 10089-10092.
- [38] J.-P. C. Ryckaert, G.; Berendsen, H., Numerical Integration of the Cartesian Equations of Motion of a System with Constraints: Molecular Dynamics of n-Alkanes, *J. Comput. Phys.* 23 (1977) 327-341.
- [39] A. Onufriev, D. Bashford, D. A. Case, Exploring protein native states and large-scale conformational changes with a modified generalized born model, *Proteins* 55 (2004) 383-94.

HIGHLIGHTS

- Linking of PTs and the active fragment provided a promising lead compound **12e**.
- Compound **12e** took a unique CE-mimicking binding mode, different with current known CETP inhibitors.
- Compound **12e** with potent CETP inhibitory activity experimentally validated our molecular modeling.
- Molecular dynamics simulations explained the detailed differences on CETP inhibitory activity between compound **12b** and **12e**.